Chapter 2

Experimental Techniques

2.1. Introduction

It will be interesting to characterize nanocrystalline materials with various techniques in order to understand the changes in their properties with respect to particle size. Various characterization techniques are employed to study the structural, electrical, optical and magnetic properties of nanomaterials. Some of the experimental techniques for characterizing the nanomaterials like Mössbauer spectroscopy, X-ray diffraction (XRD), magnetization measurements using vibrating sample magnetometer (VSM) and superconducting quantum interference device (SQUID) magnetometer, scanning electron microscopy (SEM), transmission electron microscopy (TEM) and thermogravimetric analysis (TGA) used by the author are presented in this chapter.

2.2. Experimental Techniques

2.2.1. Mössbauer spectroscopy

A brief introduction to the theory of Mössbauer effect, the various Mössbauer parameters, Mössbauer instrumentation and the method of analysis of the Mössbauer data are discussed. The phenomenon of recoilless emission and resonant absorption of nuclear gamma rays in solids is called the Mössbauer effect which was discovered by the German Physicist Rudolf L. Mössbauer during his graduate work at Heidelberg in 1957. Mössbauer effect has provided a significant contribution to the solution of a variety of problems in many branches of science, particularly in the field of solid state physics and solid state chemistry [1-6].

When a free nucleus emits radiation it undergoes recoil to conserve momentum and the energy required for the recoil comes from the emitted gamma ray itself. The recoil energy (10^{-2} eV, typical) is found to be much higher than the linewidth (10^{-9} eV, typical). As a result, the gamma ray emission line does not overlap the absorption line and nuclear resonance absorption is not observable.

If a free nucleus of mass M with two energy levels E_e and E_g separated by the transition energy E_t decays by the emission of a photon of energy E_γ, the consideration of momentum and energy yields,

$$E_R = \frac{E_\gamma^2}{2Mc^2} \text{ and } E_\gamma = E_t - E_R \tag{2.1}$$

where E_R is the system recoil energy and c is the velocity of light. Similarly, in order to excite the system from E_g to E_e we have

$$E'_\gamma = E_t + E_R \tag{2.2}$$

It is known that the excited state E_e is not sharp and has a finite width. Hence the transition energy E_t is not characterized by a single energy but by a spectral distribution $W(E)$ centered around E_t given by

$$W(E) = \frac{1}{1 + 4\left(\frac{E - E_t}{\Gamma}\right)^2} \qquad \text{with} \qquad \tau\Gamma \geq \frac{h}{2\pi} \tag{2.3}$$

where Γ is the natural line width of the excited state, τ is the mean lifetime of the nuclear level and h is the Planck's constant. The energy of the ground state is sharp (i.e. $\tau = \infty$) and hence a photon emitted in the transition from E_e to E_g has also a spectral distribution $W_s(E)$ centered around E_γ.

$$W_S(E) = \frac{1}{1 + 4\left(\frac{E - E_\gamma}{\Gamma}\right)^2} \tag{2.4}$$

A photon which would induce a transition from E_g to E_e will have a spectral distribution $W_a(E)$ centered around E'_γ and is given by

$$W_a(E) = \frac{1}{1 + 4\left(\frac{E - E'_\gamma}{\Gamma}\right)^2} \tag{2.5}$$

The resonant absorption takes place when $E_\gamma = E'_\gamma$ and it is proportional to the overlap of the above two distributions. The overlap for the atomic system is shown in Fig. 2.1.(a) and for nuclear system in Fig. 2.1.(b). It can be seen that the overlap in the latter case is very small. For resonant absorption to take place, there should be a strong overlap of emission and absorption profiles i.e. $\Gamma/2E_R$ should be greater than one. But Γ/E_R is of the order of 10^{-5} for a nuclear system and hence resonant absorption has little chance to take place under normal conditions whereas, the same is of the order of 10^3 in the case of atomic system since transition energies are 10^4 times smaller. So, the optical resonance fluorescence is readily observable.

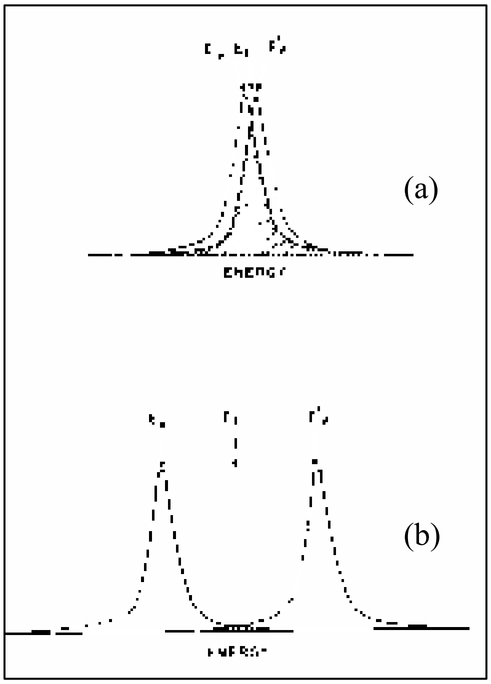

Fig. 2.1. The relationship between E_t, E_γ and E_γ' for **(a)** optical case ($E_R << \Gamma$) and **(b)** nuclear case ($E_R >> \Gamma$).

Up to this point, only freely recoiling nuclei have been considered. Mössbauer found that for nuclei bound in solids, the emitted gamma ray carries the full energy without recoil loss and resonant absorption is possible. Here the recoil momentum is taken up by the whole solid ($M_{\text{solid}} \approx 10^{22}\ M_{\text{atom}}$) and consequently, the recoil energy of the solid as a whole can be neglected. What is left is to examine the other modes by which the nucleus can transfer energy to the lattice.

There is a possibility of exciting lattice vibrations, i.e. creation or annihilation of phonons. However, the lattice vibrations are quantized and if the free atom recoil energy is less than the phonon energy, statistically, there is a fraction '*f*' of events that takes place without lattice vibrations. These events, which are called zero phonon transitions, have the spectrum centered around E_t and with the natural line width. This is called the Mössbauer effect. The recoilless fraction for an Einstein solid can be shown to be equal to $f = (1 - E_R/\hbar\omega)$ where $\hbar\omega$ is the phonon energy. For a Debye solid, it becomes

$$f = \exp\left[-\frac{3}{2}\frac{E_R}{k\theta_D}\left(1 + 4\left(\frac{T}{\theta_D}\right)^2 \int_0^{\frac{\theta_D}{T}} \frac{x}{e^x - 1}\,dx\right)\right] \tag{2.6}$$

where θ_D is the Debye temperature of the solid, T is the measurement temperature, k is the Boltzmann constant and $x = \hbar\omega/kT$.

The conditions under which the Mössbauer effect could be observed are as follows; (1) the atom (or ion) under investigation must be embedded in a crystalline lattice to avoid recoil effects and thermal broadening, (2) the gamma ray energy, E_γ must be fairly low (10 - 100 keV) so that an appreciable number of recoil free events may be obtained, (3) the life time of the excited state τ must be in the range from 10^{-11} to 10^{-6} s, (4) the internal conversion coefficient should be as small as possible, preferably less than 20, to ensure that an appreciable number of gamma transitions manifest themselves as gamma rays and not as conversion electrons and (5) the Debye temperature θ_D of the absorber should be high.

2.2.1.1. Mössbauer parameters

The hyperfine interactions i.e. interactions between a nuclear property and appropriate electronic or atomic property are of great significance yielding information regarding electronic and spin structure. There are three main hyperfine interactions; (1) electric monopole interaction (isomer shift), (2) electric quadrupole interaction (quadrupole splitting) and (3) magnetic dipole interaction (nuclear Zeeman effect). Before the discovery of Mössbauer effect, the hyperfine interaction parameters could be deduced in an indirect way. But the discovery of Mössbauer effect made it possible to study the hyperfine interactions precisely and directly with a wealth of new information. Since we are studying magnetic materials containing Fe, ^{57}Fe Mössbauer isotope is used and hence all discussions in this thesis are related to ^{57}Fe Mössbauer spectroscopy only.

2.2.1.1. (a) Isomer shift (Electric monopole interaction)

The isomer shift (I.S.) arises due to the difference in the electrostatic interaction between the nuclear charge and the electronic charge in the source and in the absorber and in the excited and ground states of the Mössbauer nucleus. This interaction causes a shift of the single resonance peak from the zero velocity position in the absence of electric quadrupole or magnetic dipole interaction as shown in Fig. 2.2. This shift is known as

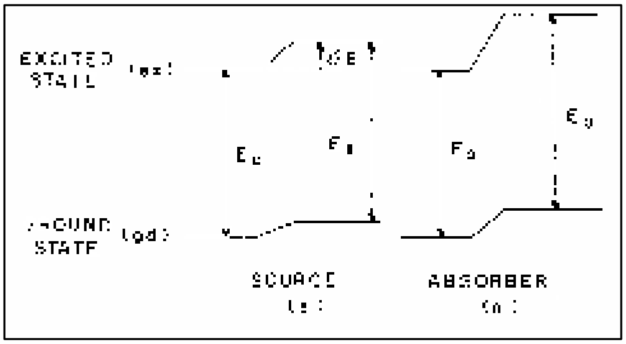

Fig. 2.2. The effect of electric monopole interaction on nuclear energy levels.

isomer shift or centre shift. When electric quadrupole and magnetic dipole interactions are present, the position of the centre of gravity of the spectrum from the zero velocity is a measure of the isomer shift. The isomer shift represents the difference in the energy change of a gamma ray relative to the point charge nucleus in the source and in the absorber during a nuclear transition between ground and excited states, viz.,

$$\text{I.S.} = [(\delta E)_e - (\delta E)_g]_a - [(\delta E)_e - (\delta E)_g]_s$$

It can be shown that

$$\text{I.S.} = (4\pi / 5)Ze^2R^2(\delta R / R)\left[\left|\Psi(0)_a\right|^2 - \left|\Psi(0)_s\right|^2\right] \qquad (2.7)$$

with $R = (R_e + R_g)/2$ and $\delta R = R_e - R_g$

where Ze is the nuclear charge, R_e and R_g are nuclear radii in its excited and ground states respectively. δR is negative for ^{57}Fe and $-e\,|\psi(0)|^2$ is the electronic charge density at the nucleus. The suffices a and s represent the terms for the absorber and source respectively.

The expression for the isomer shift can be divided into two factors. The first factor contains only the nuclear parameters which would be just a constant for studies with the same Mössbauer nucleus. The second factor contains the atomic or chemical parameter which is affected by the valence state of the atom (i.e. oxidation state of Fe) as well as the electronic configuration in the unfilled shells. The isomer shift will be influenced by the following factors: (1) any direct contribution by 4s-electrons and (2) indirect contributions from 3d^n electrons which may be considered in terms of (a) the purely ionic or non-bonding effect of a $3d^n$ configuration and (b) different σ donor and π acceptor property of surrounding ligands. In summary, one could say that the isomer shift may yield (1) the sign and magnitude of $\delta R/R$, (2) the s-electron density at the nuclear site, (3) the spin and charge states of metal ions in solids and (4) the nature of the chemical bond between the metal ion and the ligand.

2.2.1.1. (b) Quadrupole interaction

The interaction of the nuclear quadrupole moment eQ with the electric field gradient (EFG) 'eq' due to other charges in the crystal is called quadrupole interaction. The quadrupole interaction can be expressed by the Hamiltonian

$$H = \boldsymbol{Q}.\nabla\boldsymbol{E} \qquad \text{with} \quad Q_{ij} = \int \rho_n(\boldsymbol{r})\, \boldsymbol{x_i}.\boldsymbol{x_j}\, dv \tag{2.8}$$

where ρ_n is the nuclear charge density and $\boldsymbol{x_i}$ and $\boldsymbol{x_j}$ are the Cartesian coordinates of $\boldsymbol{r}$. The sign of Q_{ij} depends on the shape of the deformation of the nucleus with a negative quadrupole moment representing oblate nucleus along the spin axis and a positive moment for prolate or elongated nucleus.

The field gradient $\nabla\boldsymbol{E}$ is a 3 x 3 tensor, which could be completely represented by nine components,

$$\frac{\partial^2 V}{\partial x^2}, \frac{\partial^2 V}{\partial y^2}, \frac{\partial^2 V}{\partial x \partial y}, \frac{\partial^2 V}{\partial x \partial z}, \frac{\partial^2 V}{\partial y \partial x}, \frac{\partial^2 V}{\partial y \partial z}, \frac{\partial^2 V}{\partial z \partial x}, \frac{\partial^2 V}{\partial z \partial y} \text{and} \frac{\partial^2 V}{\partial z^2}$$

abbreviated as V_{xx}, V_{yy},V_{xy}, V_{xz}, V_{yx}, V_{yz}, V_{zx}, V_{zy} and V_{zz} respectively. Three of the off diagonal elements are dependent because of the symmetry, namely $V_{xy}= V_{yx}$, $V_{xz}= V_{zx}$ and $V_{yz}= V_{zy}$. A unique axis system of the Mössbauer atom called the principal axis of the EFG tensor can be defined such that the off diagonal elements vanish and the diagonal elements are ordered as $|V_{zz}| \geq |V_{yy}| \geq |V_{xx}|$. One diagonal element is dependent because it can be expressed in terms of the other two by the Laplace's equation $V_{zz}+V_{xx}+V_{yy} = 0$. With respect to the principal axes, the EFG tensor is described by only two independent parameters, usually chosen as $V_{zz} = eq$ and the asymmetry parameter η which is defined as

$$\eta = (V_{xx} - V_{yy})/V_{zz}$$

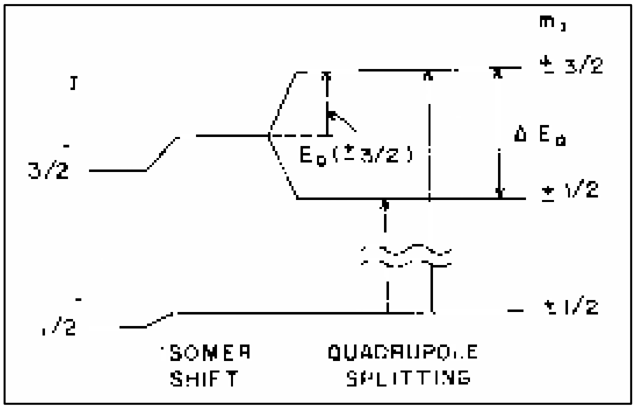

Fig. 2.3. The effect of electric quadrupole interaction on nuclear energy levels.

The eigenvalue equation for the interaction Hamiltonian can be written as

$$E_Q = \frac{e^2 qQ}{4I(2I - 1)} \left[3m_I^2 - I(I + 1)\right]\left[1 + \frac{\eta^2}{3}\right]^{1/2} \tag{2.9}$$

where the magnetic spin quantum number $m_I = I, \; I - 1, \ldots, -I$ and η is the asymmetry parameter. Hence, a nuclear state with $I > 1/2$ is $(2I + 1)$ fold degenerate and it will split into substates $|I, \pm m_I\rangle$ without shifting the centre of gravity. In the case of ^{57}Fe, the nuclear ground state with $I = 1/2$ is not split because of spherical symmetry whereas the excited state with $I = 3/2$ is split into two substates $|3/2, \pm 1/2>$ and $|3/2, \pm 3/2>$ as shown in Fig. 2.3. Hence, two resonance lines are observed and the separation between these two lines is called the quadrupole splitting. The separation (Q.S.) is given by

$$Q.S. = \left(\frac{1}{2}\right) e^2 Qq \left[1 + \frac{\eta^2}{3}\right]^{1/2} \tag{2.10}$$

The resonance lines are equal in intensity for an isotropic system. The anisotropic vibrations of the lattice (Goldanskii-Karyagin effect) give rise to asymmetric doublets. Usually, the relative intensities of the asymmetric doublets are temperature dependent. The texture effect, which arises from preferred crystal orientation, also gives rise to asymmetric doublet.

Since the quadrupole moment *eQ* is constant for a given Mössbauer nucleus, quadrupole splitting depends on the EFG. The various contributions to EFG can be represented as,

$$V_{zz} = (1 - \gamma_{\infty})(V_{zz})_{LAT} + (1 - R)[(V_{zz})_{CF} + (V_{zz})_{MO}] \tag{2.11}$$

where γ_{∞} is called the Sternheimer antishielding factor and R is Sternheimer shielding factor which represents the values arising out of antishielding and shielding of the nucleus by the core electrons respectively and $(V_{zz})_{LAT}$, $(V_{zz})_{CF}$ and $(V_{zz})_{MO}$ are contributions from lattice, crystal field and molecular orbitals. Thus, the quadrupole splitting would give information on the electronic structure, bonding and molecular symmetry.

2.2.1.1. (c) Nuclear Zeeman interaction

The interaction of the nuclear magnetic moment $\boldsymbol{\mu}$ with the internal magnetic field $\boldsymbol{H}$ at the nucleus due to atom's own electrons is called the nuclear Zeeman effect or magnetic hyperfine interaction. The Hamiltonian for this interaction can be written as

$$H_m = -\boldsymbol{\mu}.\boldsymbol{H} = -g_N\beta_N \boldsymbol{I}.\boldsymbol{H} \tag{2.12}$$

where g_N and β_N are the nuclear g factor and the nuclear magneton respectively. The energy levels are given by

$$E_m = -\mu H m_I/I = -g_N\beta_N H m_I \tag{2.13}$$

where $m_I = I, I-1, \ldots\ldots, -I$. From the eigen value equation, one can understand that there are $(2I+1)$ equally spaced energy levels and the splitting between adjacent level is $g_N\beta_N H$. The transition between the sublevels of the excited state and those of the ground state are governed by selection rules. For magnetic dipole interaction, transitions (for ^{57}Fe) with $\Delta I = 1$, and $\Delta m_I = 0, \pm 1$ are allowed giving six transitions as shown in Fig. 2.4 together with their relative intensities for a polycrystalline material where the Debye-Waller factor is assumed to be isotropic. The relative intensities are given by the square of the Clebsch-Gordon coefficients and are in the ratio 3:2:1:1:2:3 for a polycrystal as indicated in the Fig. 2.4.(a). The various contributions to the effective magnetic field could be given by

$$H = H_a - DM + (4\pi/3)M + H_S + H_L + H_D \tag{2.14}$$

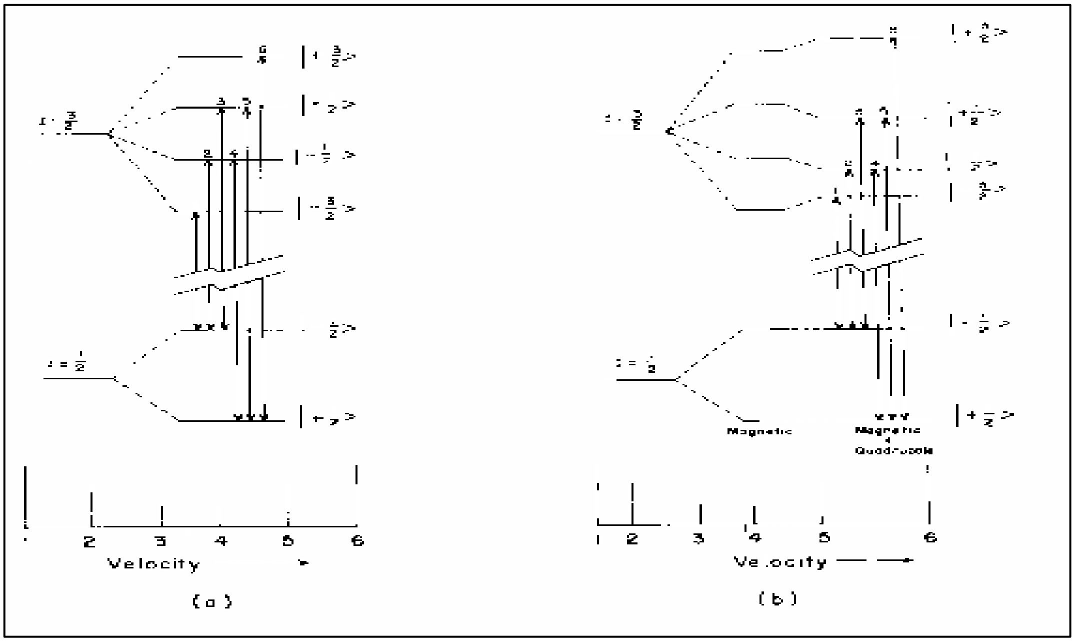

Fig. 2.4. The magnetic dipole splitting **(a)** without electric quadrupole perturbation and **(b)** with electric quadrupole perturbation.

where H_a is the external applied magnetic field, *DM* is the demagnetizing field and $(4\pi/3)M$ is the Lorentz field. These three fields would be of the order of a few Tesla (T). The Fermi contact interaction term H_S arises due to a direct coupling of the nucleus with an imbalance in the s-electron spin density at the nucleus. It is given by

$$H_S = -(16\pi/3)\ \mu_B \langle \Sigma (S\uparrow - S\downarrow) \rangle \qquad (2.15)$$

where $S\uparrow$ and $S\downarrow$ are s-electron spin densities at the nucleus with up and down spins respectively. This contribution would be of the order of 10 T for the iron group elements. The H_L refers to the contribution arising from non-zero orbital magnetic moment of the parent atom and is given by

$$H_L = -2\ \mu_B \langle r^{-3} \rangle \langle \mathbf{L} \rangle \qquad (2.16)$$

For α-Fe, this contribution is estimated to be 7 T. This term becomes zero whenever orbital angular momentum is quenched. The dipolar interaction of the nucleus with the spin moment of the parent atom is given by

$$H_D = -2\ \mu_B \langle 3\mathbf{r}\ (\mathbf{s}.\mathbf{r}/r^5) - \mathbf{s}/r^3 \rangle \qquad (2.17)$$

This contribution is estimated to be the order of 1 T. In cubic symmetry and in the absence of spin-orbit coupling, this term vanishes.

In the case of the combined effects of quadrupole and magnetic hyperfine interactions, there may be a change in the resonant line positions or line widths of the spectrum. Normally one interaction is found to be small compared to the other when they are simultaneously present. In the presence of both quadrupole and magnetic hyperfine interactions, if $e^2qQ << H$, then the eigen values are

$$E = -g_N \beta_N H m_I + (-1)^{|m_I| + \frac{1}{2}} \frac{e^2qQ}{4} \left[\frac{3\cos^2\theta - 1}{2} \right] \tag{2.18}$$

when the EFG tensor is symmetric and its principal axis makes an angle θ with the magnetic axis. The angle θ can be determined in this case.

When the EFG tensor is not axially symmetric but magnetic axis lies along one of its principal axes then the eigen values of the four excited state splittings for $I = 3/2$ are given as

$$(1/2)\, g_N \beta_N H \pm (e^2qQ/4)\, [\, (1 + 4g_N \beta_N H/e^2qQ)^2 + \eta^2/3\,]^{1/2} \tag{2.19a}$$

and

$$(-1/2\,) g_N \beta_N H \pm (e^2qQ/4)\, [\, (1 - 4g_N \beta_N H/e^2qQ)^2 + \eta^2/3\,]^{1/2} \tag{2.19b}$$

The solutions are obtained not analytically but by a full mathematical analysis using a computer. The main use of the effect of combined interactions of this type is in the determination of the sign of the EFG in polycrystalline absorbers exhibiting purely quadrupole doublets by applying an external magnetic field.

2.2.1.2. Mössbauer effect instrumentation

The purpose of the Mössbauer spectrometer is to produce a known and precise energy shift between the Mössbauer source and absorber. The method of velocity modulation of the gamma ray energy by means of Doppler effect, described by Mössbauer, provides the basis for all Mössbauer spectrometers. There are two general approaches to the measurement of gamma ray transition at different Doppler velocities:

(a) The measurement of the total number of transmitted gamma photons for a fixed time at a constant velocity, followed by subsequent counting at other velocities, in the way the spectrum is scanned step-wise is called the constant velocity spectrometer.

(b) The rapid scanning through the whole velocity range in one cycle and subsequent numerous repetitions of this scan, thereby accumulating the data for the individual velocities almost simultaneously is called the constant acceleration spectrometer. This spectrometer is widely used since it gives a continuous visual display of the spectrum which can be inspected at any time during the course of the run.

The block diagram of a constant acceleration Mössbauer spectrometer consists of a driving system (electromagnetic transducer and driving unit), digital function generator, detector, preamplifier, linear amplifier, ADC and data acquisition system with MCA and a personal computer as shown in Fig. 2.5.

The Mössbauer velocity transducer provides a precise motion to the gamma ray source during the Mössbauer experiments. The velocity transducer is based on the principle of two mechanically coupled loudspeakers, whose voice coil generates the motion, called driving coil and another coil measures the instantaneous velocity, called pick-up coil. Both the coils are rigidly mounted to a common tube and the source in turn is rigidly mounted to this tube. The frequency of the transducer is approximately 23 Hz at normal operation.

The driving coil causes motion of the transducing element as per the impressed signal from the function generator. The pick-up coil which moves in the uniform magnetic field of a Sm-Co permanent magnet, gives the information on the actual velocity to the driving unit. The difference between the impressed signal and that from the pick-up coil is proportional to the deviation of the actual velocity from its ideal value. This difference is

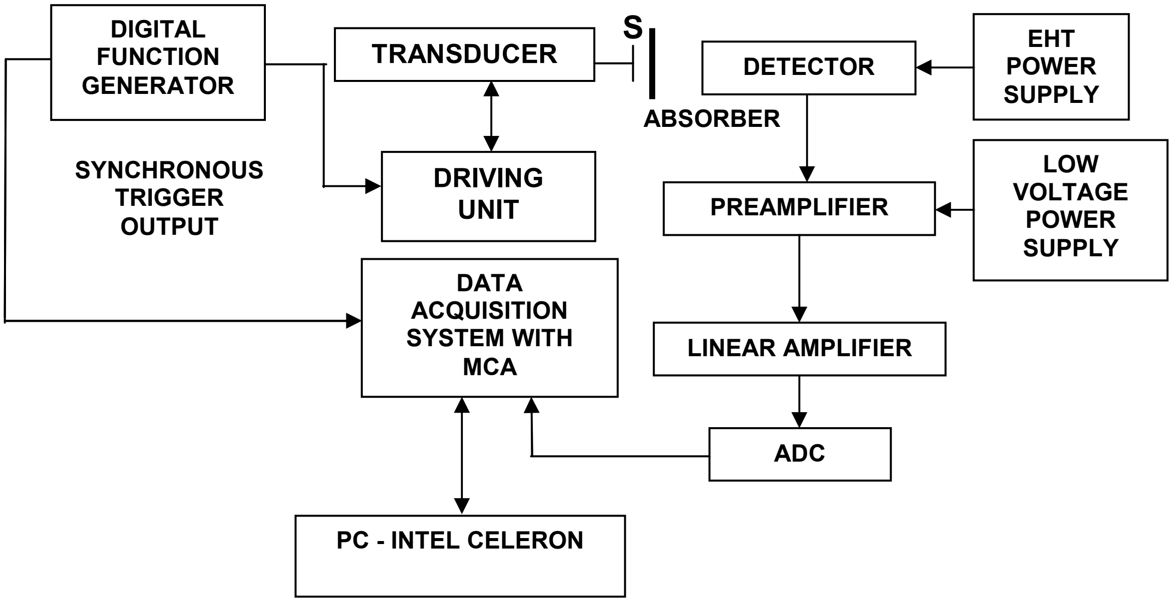

Fig. 2.5. The block diagram of a constant acceleration Mössbauer spectrometer.

amplified by the feed-back amplifier and fedback to the driving coil. Before operation, the error signal is minimised by adjusting the gain and frequency response of the feed back amplifier loop.

The digital function generator is used to provide the Mössbauer driving system with reference signal that determines the waveform of the source motion. It also provides start pulses to initiate the multichannel scaling cycle and channel advance pulse. The digital function generator can provide either a square pulse for constant velocity mode or a triangular wave for constant acceleration mode. The perfectness of the above signal controls the linearity and its frequency fixes the zero-velocity channel. The accuracy of the spectrometer depends on the accuracy and stability of the wave used.

A NaI(Tl) scintillation detector (bicron, USA) of 1 mm thickness coupled to a 38 mm diameter photomultiplier tube is used for the detection of the 14.4 keV gamma rays. The output of the detector is fed to a preamplifier. It accepts the signal directly from the detector and amplifies with minimum shaping in such a way that the maximum signal to noise ratio is preserved. The output of the preamplifier is fed to the linear amplifier in order to amplify and shape the detector output.

The multichannel analyser (MCA) is a versatile instrument for acquiring data of one or several experiments in multichannel scaling (MCS) or pulse height analysis (PHA) mode. This system has two memories with 4096 channels for acquiring data of two independent spectra. In one of the memories, the PHA spectrum of ^{57}Co is stored and in the other, Mössbauer spectrum of the sample is recorded. The contents of the memories can be continuously transferred to the computer. The PC -Pentium-II with RS-232 interface is used as an intelligent terminal for controlling the functions of MCA and for displaying the acquired spectrum. The functions of the MCA are completely controlled by the computer.

The author has used a Wiessel constant acceleration Mössbauer spectrometer with a Co^{57}/Rh source of strength 925 GBq kept at 300 K. The CMCA software supplied along with the system, apart from data transfer, has several other provisions like, spectrum folding, zooming particular region and automatic data storage into hard disk at a particular interval etc. The software is user-friendly and driven by the soft key operation. The spectrometer calibration is checked before and after the measurements with a natural iron foil at 300 K. The linearity of the spectrometer is accurate within one channel with 22 - 25 % absorption for the natural iron absorber. The linewidth of the natural iron absorber is 0.28 mm/s for the outer lines of the ^{57}Fe Mössbauer spectrum. The samples in suitable quantity are mixed with boron nitride powder and wrapped in an aluminium foil and the spectrum is recorded in transmission geometry. The low temperature measurements up to 16 K were performed using a CTI, USA make closed cycle helium refrigerator. The temperature stability of the measurements is ± 0.2 K.

2.2.1.3. Analysis of the Mössbauer spectrum

The Mössbauer spectra for the crystalline samples are least-squares fitted with Lorentzian lines for discrete fields. A Mössbauer spectrum, in general, consists of a sum of Lorentzians if the relaxation effects are not present. The versatile program developed by Bent *et al.* [7] has been used to fit the data by the least-squares method.

The theoretical function which is fitted to the experimental spectrum depends on a number of input parameters. These are varied in the fitting procedure to obtain a minimum in the value of Q^2, which is a statistically weighted sum over all data points of the squares of the difference between the postulated function and the experimental data. Its explicit form is,

$$Q^2 = \sum_{k=1}^{n} \frac{1}{y_k}\left[F(x_k; \alpha_1, \ldots \alpha_j, \ldots \alpha_p) - y_k\right]^2 \tag{2.20}$$

$F(x_k, \alpha)$ is the value of the postulated function evaluated at k^th data point and y_k is the number of counts in the same velocity channel. The function is determined by the variable parameters α_j and the spectrum consists of n data points. The velocity at each point is denoted by x_k. The function is linearised by truncating its Taylor expansion to give,

$$F(x_k, \alpha) = F(x_k, \alpha^0) + \sum_j \left[\frac{\partial F(x_k, \alpha^0)}{\partial \alpha_j}\right]_{\alpha = \alpha^0} \left(\alpha_j - \alpha_j^0\right) \tag{2.21}$$

which may be written in the abbreviated form,

$$F_k = F_k^0 + \sum_j \left[\frac{\partial F_k^{\alpha}}{\partial \alpha_j}\right] \Delta\alpha_j$$

The fit is started by estimating the value of α_j^0 from the experimental spectrum. Then the adjustments, $\Delta\alpha_j$, required for Q^2 to be minimum are approximated by the solution of the normal equations,

$$\sum_{j,k} \frac{1}{y_k} \frac{\partial F_k^0}{\partial \alpha_i} \frac{\partial F_k^0}{\partial \alpha_j} \Delta \alpha_j = \sum_{k} \left[\frac{F_k - y_k}{y_k} \right] \frac{\partial F_k^0}{\partial \alpha_i}$$

These equations are more conveniently expressed in the matrix form,

$$\sum_j (AM)_{ij} \Delta\alpha_j = (BM)_i$$

where *AM* is the measurement matrix and *BM* is the data vector.

The function F_k designed to fit the Mössbauer data is not linear in α_j and therefore the solution of above equation will not immediately yield the minimum Q^2. In general the new parameter values $\alpha_j^0 + \Delta\alpha_j$ will give a value of Q^2 which is smaller than the previous value. If Q^2 continues to decrease, the iterations are repeated until the changes, $\Delta\alpha_j$ becomes negligibly small. The final smallest value of Q^2 is normalised by dividing the number of degrees of freedom to give the value of χ^2 for the fit. The function $F(x_k, \alpha)$ is given by

$$F(x_k, \alpha) = B \left[1 + \left(\frac{\sigma x_k}{100V} \right) - \left(\frac{2A}{100\,\pi} \right) \sum_{j=1}^{N} \frac{h_j}{w_j + (4/w_j)(x_k - e_j)^2} \right] \qquad (2.22)$$

where B is the background level of the spectrum, σ is a measure of the slope of the background, V is the peak to peak velocity used in the experiment and A is the total area of the spectrum measured in units of velocity times the percentage of the background. The quantities h_j, w_j and e_j represent the relative intensity, width and velocity position respectively of the jth line. α represents the parameter varied in the fitting procedure to get minimum Q^2. The quantities x_k and N do not vary and are determined by the input.

The above least-squares program has many flexible options such as to vary the line intensities or to calculate the intensities internally or to prefix certain input parameters. The widths of all spectral lines of a sextet or the width of any one spectral line of a sextet can be varied independently or prefixed.

2.2.3. X-ray diffraction (XRD)

Powder XRD is used widely to identify the crystal structure of a material. In addition, XRD is also used to find the average grain size, lattice parameters, quantitative and qualitative phase analysis and to determine lattice strains. A comprehensive review on the use of powder XRD for the characterization of materials is presented in the literature by Langfordy and Louër [8]. In the characterization of nanomaterials using XRD, the average grain size has been usually calculated from the Debye-Scherrer equation [9]

$$d = \frac{0.9\lambda}{\beta\cos\theta} \tag{2.23}$$

where λ is the wavelength of the radiation used, β is the full-width at half-maximum of the peak after fitting it with a Lorentzian and θ is the angle at which the peak occurs. A pseudovogit function is used to fit the peak when the line broadening is very large. The r.m.s. strain is calculated using the relation [10]

$$< e^2 >^{1/2} = \frac{\beta_e}{2\eta\tan\theta} \tag{2.24}$$

where β_e is the full-width at half-maximum of the X-ray peak and η is the coefficient which depends on the distribution of strains and it is chosen as unity assuming uniform distribution of strains and θ is the angle of diffraction.

The author has used RIGAKU and JEOL X-ray diffractometers with Cu and Fe targets respectively. The instrumental line broadening checked using a Si standard is found to be negligible. The XRD is recorded in full time mode with a count time of 20 s. For the analysis of the X-ray data, standard analysis softwares are used for fitting the peaks and for the calculation of the lattice constants. The identification of the phases is carried out using the JCPDS powder diffraction reference (PCPDFWIN version 2.02).

2.2.4. Vibrating sample magnetometer (VSM)

When a sample is placed in a uniform magnetic field, a dipole moment is induced proportional to the product of the applied field and the susceptibility of the sample. In a vibrating sample magnetometer, the sample is made to undergo sinusoidal motion which induces an electrical signal in the pick-up coils. This signal is proportional to the magnetic moment of the sample, the amplitude of vibration and frequency of the signal. The magnetometer separates the other signals from that of the sample's magnetic moment to obtain the net magnetic moment.

The VSM consists of a head assembly for the sinusoidal motion of the drive, the sample rod, electromagnet assembly, controller and a computer [11]. The transducer in the head assembly, a loud speaker, converts a sinusoidal a.c. drive signal of frequency normally 84 Hz, into a vertical vibration of the sample rod. The sample is normally placed at the other end of the rod which is placed in between the pole pieces of an electromagnet. The coils mounted on the pole pieces of the electromagnet pick up the signal resulting from the sample motion. A vibrating capacitor beneath the transducer generates an a.c. control signal proportional to the vibrational amplitude and frequency. This signal is fed back to the oscillator where it is compared with the drive signal and also it is phase-adjusted and routed to the signal demodulator where it functions as the reference drive signal. The signal from the sample is also buffered, amplified and applied to the demodulator. There it is demodulated with respect to the reference signal from the moving capacitor assembly. The resulting signal gives the sample's magnetic moment alone. The VSM controller connected to a computer measures the magnetic moment vs. field value of the sample which is obtained after calibration. The schematic diagram showing the position of the sample, the hall probe for measuring the magnetic field and the pick up coil for measuring the magnetic moment is shown in Fig. 2.6.

Fig. 2.6. The block diagram of a VSM.

The VSM is calibrated with a Ni standard before the measurements to give a saturation magnetization of 55 ± 0.5 A m^2/kg at 0.5 T. The sample is placed at the centre of the pole pieces by adjusting the sample rod in the X, Y and Z directions. The magnetic moment is adjusted to be maximum at the X and Z directions and minimum along the Y direction (along the axis of the magnet) during calibration. High temperature measurements were performed in a sample holder made of boron nitride or quartz. The sample cups are cleaned with nitric acid or hydrochloric acid solutions and the contribution due to impurity is avoided by verifying the magnetic signals from the empty cups. The author has used a EG&G PARC (Model 4500) VSM for fields up to 0.7 T and a Tamakawa make (TM-VSM1230-HHHS, Japan) VSM for fields up to 2 T at room temperature. The sensitivity of the VSM is 10^{-3} A m^2 and a suitable amount of the sample is chosen so that the magnetic moment is around 1 to 10^{-2} A m^2. A high temperature oven was attached to the VSM for measurements above room temperature which was evacuated to a pressure of less than 10^{-4} mbar. For low temperature measurements up to 77 K, a cryostat attached to the VSM was cooled by pouring liquid nitrogen. The hysteresis loop measurements were performed after the temperature stabilized at the set temperature. The pole pieces of the Tamakawa VSM are changed to accommodate the low temperature and high temperature attachments and a maximum field of 1 T is attained.

2.2.5. Superconducting quantum interference device (SQUID) magnetometer

When a sample is moved through superconducting detection coils, at a given temperature and in a homogenous magnetic field, the magnetic moment of the sample induces an electric current in the detection coils. Since the coils, consisting of the connecting wires and the SQUID input coil, form a closed superconducting loop, this current is not damped and any change in magnetic flux in the detection coils produces a proportional change in the persistent current in the detection circuit. Thus, by moving the sample from one side of the gradiometer to the other, a flux integration is performed. A flux transformer allows to transmit the gradiometer signal to the SQUID. The only instrument with the highest sensitivity for magnetic measurements is the SQUID magnetometer which can measure magnetic fields of the order of femtotesla (10^{-15} T) and magnetic moments of the order of 10^{-10} A m^2 [12]. When a superconducting ring interrupted by a weak link is exposed to an external magnetic field, a shielding supercurrent flows around the inner surface of the ring via the weak link. The supercurrent will be an oscillating function of the magnetic field intensity, such that it first rises to a peak as the field increases, then falls to zero, increases again and so on. In a SQUID, these periodic variations are exploited to measure the current in the superconducting ring and, hence, the applied magnetic field. The components of a SQUID magnetometer are shown in Fig. 2.7.(a) and Fig. 2.7.(b) shows the schematic diagram of the SQUID magnetometer assembly. The SQUID magnetometer consists of mainly four parts described below (i) a detection coil, which senses changes in the external magnetic field and transforms them into an electrical current, (ii) an input coil which transforms the resulting current into a magnetic flux in the SQUID sensor, (iii) electronics which transform the applied flux into a room temperature voltage output and (iv) acquisition hardware and software for acquiring, storing and analyzing data. Both the SQUID amplifier and the detection coils are superconducting devices. Thus some type of refrigerant or refrigeration device is needed to maintain the SQUID and detection coil in the superconducting state. In this work a magnetic particle measurement system (MPMS) Quantum Design SQUID magnetometer was used for high field measurements up to 7 T with the lowest measured temperature down to 5 K. The sample weight is chosen to be around 20-30 mg so that any error in the magnetic measurements due to error in the measurement of weight would be negligible.

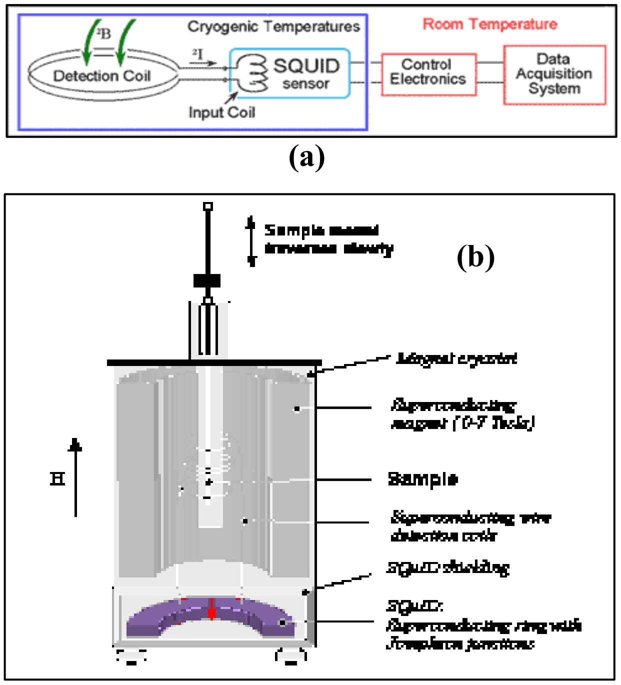

Fig. 2.7. (a) The schematic block diagram of a SQUID and **(b)** the schematic diagram of the SQUID magnetometer assembly.

2.2.6. Scanning electron microscope

Electrons from a thermionic or field-emission cathode are accelerated by a voltage of 1-50 keV. The smallest beam cross-section at the gun is demagnified by a two or three stage electron lens system, so that an electron probe of diameter 0.1-1µm is formed at the specimen surface. By changing the excitations of the first condenser lens and the objective aperture in the obective lens as shown in Fig. 2.8, the electron probe current, aperture and size can be varied [13]. The image construction in the SEM is accomplished by mapping the intensity of one of the secondary electron or backscattered electron signals from the specimen onto a viewing screen or film. There is a point-to-point transfer of this intensity information, since the SEM scan generator simultaneously drives an electron beam across the surface of the specimen and an electron beam on the viewing cathode-ray tube (CRT) or recording device. The scan coils in front of the objective lens scans the electron probe in a raster across the specimen and in synchronism with the electron beam of a separate CRT. The intensity of the CRT is modulated by the signals recorded to form the image. The block diagram of the SEM image formation system is shown in Fig. 2.9. In the present studies a Hitachi (S-4100) SEM is used to examine the morphology of the particles after dispersing it in a carbon tape.

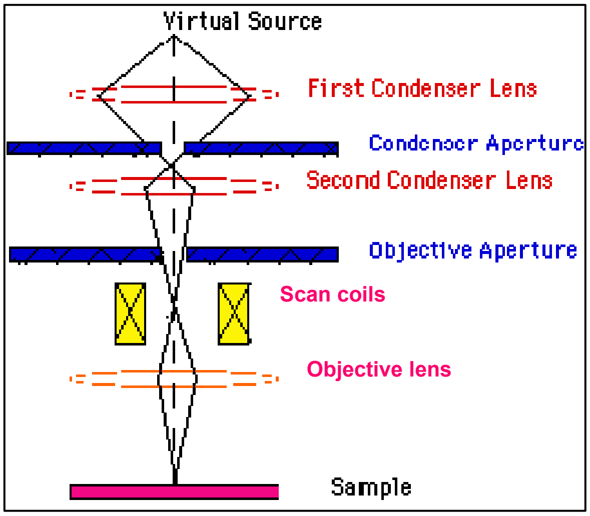

Fig. 2.8. The schematic diagram representing the arrangement of the lenses and image formation in a SEM.

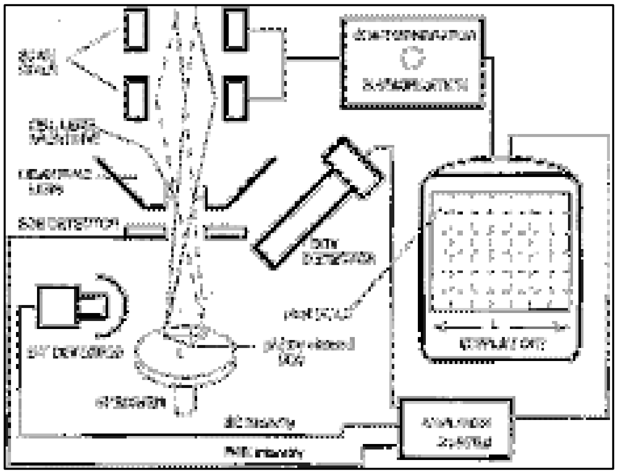

Fig. 2.9. The block diagram showing the SEM image formation in a display unit [14].

2.2.7. Transmission electron microscope

The electrons from the electron gun are accelerated to a very high voltage (100-200 keV) which are allowed to pass through a specimen and focusing lenses. The lens-systems consist of electronic coils generating an electromagnetic field. The ray is first focused by a condenser. It then passes through the specimen, where it is partially deflected. The degree of deflection depends on the electron density of the specimen. The greater the mass of the atoms, the greater is the degree of deflection. If the intermediate lens shown in Fig. 2.10 is adjusted so that its object plane is the image plane of the projector lens, then an image is projected on to the viewing screen. If the back focal plane of the objective lens acts as the object plane for the intermediate lens, then the diffraction pattern is projected in the viewing screen [15]. The TEM has the advantage that it is able to resolve to the order of a few Å. In this work a Hitachi (HF-2000) High Resolution Transmission Electron Microscope (HRTEM) is used to study the morphology of the nanoparticles with a resolution of 2 - 3 Å. The samples were examined under the TEM after dispersing them in methanol and placing a few drops of the mixture in the Cu grid.

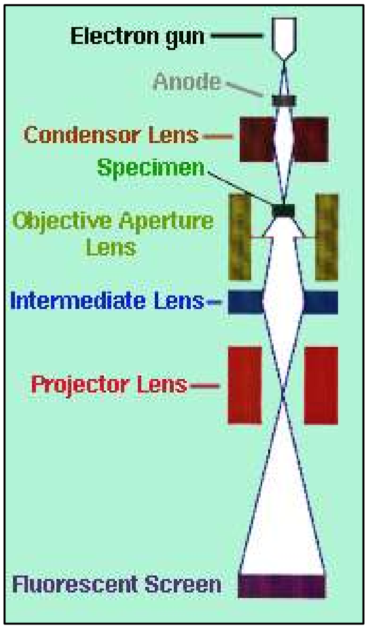

Fig. 2.10. The schematic diagram representing lenses and image formation in a TEM.

2.2.8. Thermogravimetric analyzer (TGA)

The thermal measurements are employed to determine the various phenomena occurring in a material like phase transition, melting, crystallization, glass transition and decomposition [16]. The thermal measurement instrument like, thermogravimetric analyzer, is used to find the weight loss and Curie transition in a sample.

In thermogravimetric analysis, the mass of a sample in a controlled atmosphere is recorded continuously as a function of temperature or time as the temperature of the sample is increased. The thermogravimetric analyzer consists of a sensitive analytical balance to measure the weight accurately, a micro-furnace to change the temperature in a controlled fashion at a specified rate, a purge gas system for providing an inert atmosphere and a microcomputer for the instrument control. The author has used Perkin Elmer TGA 7 PC Series thermogravimetric analyzer for measuring the Curie temperature of the samples by placing a small magnet around the micro-furnace producing a field of 4 mT. Before starting the experiment, the instrument is calibrated with standard Ni and Fe with the known Curie transition [17].

2.3. Conclusion

The various experimental techniques, for the characterization of the materials, like X-ray diffraction, magnetization measurements, scanning electron microscopy, transmission electron microscopy and thermogravimetric analysis techniques are briefly described. The theory of Mössbauer effect and the Mössbauer parameters, the Mössbauer instrumentation and the analysis of the Mössbauer data have been discussed in detail.

References

[1] N. N. Greenwood and T. C. Gibb, *Mössbauer Spectroscopy* (Chapman and Hall, London, 1971).

[2] G. K. Wertheim*, Mössbauer Effect: Principles and Applications* (Academic Press, New York, 1964).

[3] V. G. Bhide, *Mössbauer Effect and its Applications* (Tata McGraw Hill, New Delhi, 1973).

[4] R. L. Mössbauer and M. J. Clauser, in *Hyperfine Interactions,* Eds. A. J. Freeman and R. B. Frankel, (Academic Press, New York, 1967) p. 498.

[5] G. M. Bancroft, *Mössbauer Spectroscopy: An Introduction to Inorganic Chemists and Geochemists* (McGraw Hill, U.K., 1973).

[6] V. I. Goldanskii and R. H. Herber, *Chemical Applications of Mössbauer Spectroscopy* (Academic Press, New York, 1968).

[7] M. F. Bent, P. Persson and D. G. Agresti, Computer Phys. Commun. **1** (1969) 67.

[8] J. I. Langford and D. Lauër, Rep. Prog. Phys. **59** (1996) 131.

[9] B. D. Cullity, *Elements of X-ray Diffraction* (IInd Ed.) (Addison-Wesley, Ontario, 1977).

[10] J. Friedel, *Dislocations* (Pergamon, Oxford, 1964).

[11] VSM Model 4500, *User's Manual*, EG&G PARC, USA (1987).

[12] A. E. Mahdi, L. Panina, and D. Mapps, Sensors and Actuators A **105** (2003) 271.

[13] P. W. Hawkes, Ed., *SEM- Physics of Image Formation and Analysis, Springer Series in Optical Sciences* (Springer-Verlag, 1984)Vol. 45.

[14] G. W. Chandler and S. Seraphin, in *Materials Research and Methods*, Ed. E. N. Kaufmann, (John Wiley and Sons, Inc., New York, 2000) Chap. 11.

[15] D. B. Williams and C. B. Carter, *Transmission Electron Microscopy* (Plenum Press, New York, 1996).

[16] W. Wesley, M. Wendlandt, *Thermal Analysis* (John Wiley and Sons, New York, 1964).

[17] *TGA - 7 Thermogravimetric Analyser* - User's manual, Perkin-Elmer Inc., USA 1989.